Writhing instabilities of twisted rods: from infinite to finite length

S. Neukirch*, G.H.M. van der Heijden and J.M.T. Thompson
Centre for Nonlinear Dynamics and its Applications
University College London
Gower Street, London WC1E 6BT, U.K.

October 23, 2001

Abstract

We use three different approaches to describe the static spatial configurations of a twisted rod as well as its stability during rigid loading experiments. The first approach considers the rod as infinite in length and predicts an instability causing a jump to self-contact at a certain point of the experiment. Semi-finite corrections, taken into account as a second approach, reveal some possible experiments in which the configuration of a very long rod will be stable through out. Finally, in a third approach, we consider a rod of real finite length and we show that another type of instability may occur, leading to possible hysteresis behavior. As we go from infinite to finite length, we compare the different information given by the three approaches on the possible equilibrium configurations of the rod and their stability. These finite size effects studied here in a 1D elasticity problem could help us guess what are the stability features of other more complicated (2D elastic shells for example) problems for which only the infinite length approach is understood.

Keywords : **stability and bifurcations, buckling, finite deflections, elastic material, beams and columns**

1 Introduction

We study equilibrium solutions of long and thin elastic rods (or filaments). We use the Cosserat rod theory [1] to describe the state of the rod by its center line together with the

*corresponding author : s.neukirch@ucl.ac.uk / Tel: +41 21 693 29 06 / Fax: +41 21 693 42 50

field of directors. At each point along the center line curve, a set of 3 orthogonal vectors, the directors, provides a way to describe local bending, twisting, stretching and shearing of the elastic material. Constitutive relations express the way these elastic deformations are related to the stress applied to the rod.

We first recall the equilibrium equations of an unshearable, inextensible rod with symmetric cross section and linear constitutive relations, namely an elastica. Then our goal is to examine static configurations (and their stability) of a rod clamped at both ends (see fig. 1).

The force and moment balance equations for an infinitesimal cross-section element of the rod are given by [1]:

$$\boldsymbol{F}' = \boldsymbol{0}, \tag{1}$$

$$\boldsymbol{M}' + \boldsymbol{R}' \times \boldsymbol{F} = \boldsymbol{0}, \tag{2}$$

where $(\,)' \stackrel{\text{def}}{=} d/dS$, S denoting arclength along the rod. Let $\{\boldsymbol{d}_1, \boldsymbol{d}_2, \boldsymbol{d}_3\}$ be a right-handed rod-centred orthonormal co-ordinate frame with $\boldsymbol{d}_3$ the local tangent to the rod and $\boldsymbol{d}_1$ and $\boldsymbol{d}_2$ two vectors in the normal cross-section that enable us to follow the twist as we travel along the rod. In the case of an inextensible, unshearable rod we have :

$$\boldsymbol{R}' = \boldsymbol{d}_3, \tag{3}$$

while the evolution of the co-ordinate frame $\boldsymbol{d}_i$ along the rod is governed by the equation :

$$\boldsymbol{d}_i' = \boldsymbol{u} \times \boldsymbol{d}_i \qquad (i = 1, 2, 3). \tag{4}$$

Here $\boldsymbol{u}$ is the strain vector whose components in the moving frame are the curvatures and the twist. For a naturally straight and prismatic rod, we introduce linear constitutive relations between the moments and the strains as follows:

$$\boldsymbol{M} \cdot \boldsymbol{d_1} = EI_1 \boldsymbol{u} \cdot \boldsymbol{d_1}, \quad \boldsymbol{M} \cdot \boldsymbol{d_2} = EI_1 \boldsymbol{u} \cdot \boldsymbol{d_2}, \quad \boldsymbol{M} \cdot \boldsymbol{d_3} = GJ \boldsymbol{u} \cdot \boldsymbol{d_3} \tag{5}$$

where E is Young's modulus of elasticity, I_1 and I_2 are the moments of inertia about $\boldsymbol{d}_1$ and $\boldsymbol{d}_2$, respectively, while G is the shear modulus and J the polar moment of inertia. We will consider rods with symmetrical cross section i.e. $I_1 = I_2$. We have then 7 unknown vector functions $\boldsymbol{F}$, $\boldsymbol{M}(S)$, $\boldsymbol{R}(S)$, $\boldsymbol{d}_1(S)$, $\boldsymbol{d}_2(S)$, $\boldsymbol{d}_3(S)$, $\boldsymbol{u}(S)$ and 6 vectorial ordinary differential equations (1)–(4) and a set of three algebraic equations (5) relating them. A static configuration will be locally stable if it represents a local minimum of the potential energy with regard to all adjacent admissible virtual configurations satisfying the boundary conditions.

The clamped boundary conditions used here (see fig. 1) can be written as :

$$\boldsymbol{d}_3(A) = \boldsymbol{d}_3(B) \tag{6}$$

$$\boldsymbol{R}(B) - \boldsymbol{R}(A) = \lambda\, \boldsymbol{d}_3(B) \text{ with } \lambda \in \mathbb{R} \tag{7}$$

We will call end-rotation R the total angle by which the end A is turned around the axis $\boldsymbol{\ell}$. We will call end-shortening D the difference between the length of the rod and the signed distance $\overline{AB}$ (see eq. (9) for a precise definition). We are interested in two types of experiments :

- Fixed-R experiment : we start with a twisted straight rod in which we have put a certain number of turns, then we gradually move the two ends in without turning them. During such an experiment the twist rate $\boldsymbol{u} \cdot \boldsymbol{d_3}$ and hence the twisting moment $\boldsymbol{M} \cdot \boldsymbol{d_3}$ will adapt passively.

- Fixed-D experiment : we start with a configuration in which the two ends are at a certain distance from each other and then we gradually turn the two ends without changing that distance. During such an experiment the tension in the rod $\boldsymbol{F} \cdot \boldsymbol{d_3}$ will adapt passively.

2 The infinite length case

In our first approach, the rod is assumed to be of infinite length. We denote the (tensile) magnitude of the force vector by T and the projection of the moment $\boldsymbol{M}(S)$ along the tangent of the rod $\boldsymbol{R}'$ by M. Using (1–5), we find that this twisting moment M is constant along our symmetrical rod. It is then equal to the applied twisting moment at point B.

We want to find all the possible configurations for all values of the loads M and T. We make use of the Kirchhoff analogy [1] in which a configuration of the rod is associated with a trajectory in the phase space of the related dynamical system (eqs. (1)–(4)). A rod of infinite length has to be associated with a trajectory of infinite time-length relating two points in the phase space. These two points have to fulfil boundary conditions. For clamped boundary conditions (6) and (7), only the trivial equilibrium point corresponding to a straight rod and the homoclinic trajectory associated with it are acceptable trajectories [8, 3]. Furthermore, properties of this homoclinic solution show that the force vector must be along the $\boldsymbol{\ell}$ axis [8]

A linear analysis reveals a subcritical pitchfork bifurcation when the condition

$$M^2 = 4\,E\,I\,T \tag{8}$$

is satisfied [8]. At this point the straight configuration loses stability and a branch (surface) of non-trivial solutions bifurcates from the trivial one. These non-trivial solutions correspond to a rod deforming in $3D$.

In this section, we replace M and T by $M \to \frac{M}{EI}$ and $T \to \frac{T}{EI}$ respectively, in order to eliminate EI.

The end-to-end distance of an infinite rod is of course infinite in both the trivial and non-trivial configuration. However, since we are dealing with a homoclinic orbit we can define the end-shortening of the rod by taking the end-shortening, D, of a finite rod defined by

$$D \stackrel{\text{def}}{=} L - \boldsymbol{R}'(B) \cdot (\boldsymbol{R}(B) - \boldsymbol{R}(A)) \tag{9}$$

and letting the length L tend to infinity. The result is [17, 3] :

$$D = \sqrt{\frac{16}{T}\left(1 - \frac{M^2}{4T}\right)} \tag{10}$$

As the rod deforms in 3D, we can follow the angle made by the tangent $\boldsymbol{R}'(S)$ of the rod and the axis $\boldsymbol{\ell}$: $\cos\theta(S) \stackrel{\text{def}}{=} \boldsymbol{R}'(S) \cdot \boldsymbol{u}_{\boldsymbol{\ell}}$ ($\boldsymbol{u}_{\boldsymbol{\ell}}$ being a unit vector in the direction $\boldsymbol{\ell}$). The symmetries of the problem imply that this angle $\theta(S)$ is maximum at the middle of the rod and this maximum value is given by [17, 3] :

$$M^2 = 2\,T\,(1 + \cos\theta_{max}) \tag{11}$$

Eq. (11) describes the post-buckling surface of an infinite twisted rod, i.e. all possible values of the loads M and T together with the deflection θ_{max}. This surface is drawn in fig. 2 which supplies all the information we need for our infinite rod. For all values of M, T there exists a straight configuration ($\theta(S) \equiv 0$ hence $\theta_{max} = 0$). For $M^2 < 4T$, due to the subcriticilaty of the bifurcation at $M^2 = 4T$, there is also a buckled configuration. Under dead loading (controlled T and M) the straight configuration is stable when $M^2 < 4T$; and unstable when $M^2 > 4T$, in which case the rod jumps to self-contact. Meanwhile the buckled configuration is always unstable (the perturbed rod dynamically either returns to a straight configuration or jumps to self-contact). To define self-contact, we need to introduce the radius ρ of the rod. Self-contact occurs on a buckled rod when two center line points P_1 (at $\boldsymbol{R}(S_1)$) and P_2 (at $\boldsymbol{R}(S_2)$) approach each other at a minimum distance of twice the radius ρ : $d(P_1P_2) = 2\rho$ and $(\boldsymbol{R}(S_2) - \boldsymbol{R}(S_1)) \cdot \boldsymbol{R}'(S_1) = 0$ and $(\boldsymbol{R}(S_2) - \boldsymbol{R}(S_1)) \cdot \boldsymbol{R}'(S_2) = 0$ (see also [15, 7, 5]).

We are here interested in rigid loading : slowly tuning end-shortening and end-rotation and letting M and T adapt passively. The static configurations will be the same as in dead loading, but their stability will not. Since the rod is considered infinitely long, we cannot really control end-rotation (which in this case would be infinite as soon as $M \neq 0$). Hence constant R has to be interpreted as constant M. We have plotted in

fig. 2 curves of constant end-shortening D and of constant twisting moment M lying on the post-buckling surface described by (11). As we go from infinite to finite length, this degeneracy between R and M will disappear.

Fixed-R experiment : using the results derived in this section, we shall now describe what happens in a typical fixed end-rotation experiment. We start with a straight unstressed ($T = 0, M = 0$) rod. We put it under pure tension ($T > 0, M = 0$). Then we start to twist it ($M > 0$) while staying under the buckling load ($M^2 < 4T$) : suppose we have reached point E in fig. 3. Then we try to make the rod buckle by pushing its two ends together without rotating them (so we will stay at the same value of $M = M_E$). First the tension will decrease, but the rod will stay straight until we reach point F, where buckling is initiated. From F, the path follows the post-buckling surface. The rod is now buckled in $3D$, which means $\theta_{max} > 0$. From (11) it follows that T starts to increase again. Our constant $M = M_{EFG}$ path will cross curves of constant end-shortening and eventually reach point G, where the curve $D = D_2$ is tangent to the line GF. At that point the end-shortening has a maximum (if we were to go further along the path $M = M_{EFG}$, D would in fact decrease). We have reached a fold and the remainder of the line $M = M_{EFG}$ is unstable. If we try to increase the end-shortening from G, keeping M constant, the rod will jump to self-contact. At the jump point G, where the curves are tangent, we have $\frac{\partial D}{\partial T} = 0$ i.e. $M^2 = 2T$. Putting this into eq. (11) yields $\theta_{max} = \frac{\pi}{2}$. So the jump occurs when the middle of the rod has its tangent perpendicular to $\boldsymbol{AB}$.

Finally, we note that in this infinite length case, there will be a jump to self-contact (happening for large enough D) for any twisting moment M.

3 'Semi-finite' correction

As pointed out in the previous section, the main problem of the infinite length case is that as soon as the twisting moment M is non-zero, the end-rotation is infinite. So we will

now consider a rod of finite length, but still long enough to associate the configuration with the homoclinic orbit in the phase space. Such a study has been performed in [3] but more recently an approximate formula for the end-rotation has been derived in [8] by integrating over most of the homoclinic trajectory :

$$R = \frac{ML}{GJ} + 4 \arccos \frac{M}{2\sqrt{EIT}} \tag{12}$$

where GJ is the torsional stiffness of the rod. The first term on the right hand side of eq. (12) is just the total twist and the second term stands for the writhe, a measure of the out-of-plane deformation of the rod [8]. The presence of the length L in the total twist in (12) explains why when the length is increased to infinity the end-rotation tends to infinity. It also sheds light on the degeneracy of R and M when $L = \infty$: when L becomes very large, eq. (12) becomes : $R \sim \frac{ML}{GJ}$ and constant R is just like constant M. Meanwhile, the end-shortening is still given by (10).

Since L is finite we can introduce normalized variables : $m = ML/EI$, $t = TL^2/EI$, $d = D/L$, $\gamma = GJ/EI$. Eqs. (11), (10) and (12) can then be written :

$$m^2 = 2\,t\,(1 + \cos\theta_{max}) \tag{13}$$

$$d = \sqrt{\frac{16}{t}\left(1 - \frac{m^2}{4t}\right)} \tag{14}$$

$$R = \frac{m}{\gamma} + 4 \arccos \frac{m}{2\sqrt{t}} \tag{15}$$

We see that constant end-rotation R no longer means constant twisting moment m. We also remark that the eqs (13)–(15) depend on the bending and torsional stiffnesses EI and GJ only through γ in the equation for R. Therefore, the post-buckling surface (again given by fig. 2), in terms of nondimensionalized coordinates, does not depend on γ, but the stability results will. We will plot results for $\gamma = \frac{5}{7} \simeq 0.71$ which is the value of the stiffness ratio for Nitinol rods which we have used in experiments [4]. This value

of γ corresponds to the value for the Poisson's ratio ($\nu = \gamma^{-1} - 1$) of a solid circular cross-section hard rubber rod as given in [2] : $\nu = 0.4$.

Taking into account this new equation for R, we can draw a semi-finite correction to fig. 3. In fact, only curves of constant end-rotation will change and indeed we see in fig. 4 that these curves are no longer lines of constant m. Each of these curves starts on the buckling line ($m^2 = 4t$). With decreasing m, the ones with large R are all ending at $t \to +\infty$, whereas the curves with small R are all ending at $(m, t) = (0, 0)$. The figure is thus divided into two different regions by the constant end-rotation curve $R = 2\pi$ that ends at the point $(m, t) = (0, 4\gamma^2)$. At this point $d = \frac{2}{\gamma}$. This special curve is drawn bold in fig. 4.

The two different regions of fig 4 are :

-1- the first region, above the $R = 2\pi$ curve (bold), where increasing end-shortening while keeping end-rotation fixed will bring a loss of stability when the curves of constant end-shortening and constant end-rotation are tangent. At this point we have :

$$m^2 = 4\,t\,\left(1 - \frac{\left(\gamma + \sqrt{\gamma^2 + 2\,t}\right)^2}{4\,t}\right) \tag{16}$$

This curve is drawn dashed in fig. 4. It is easy to check that at this point of instability we always have $m^2 < 2t$, which means from eq. (13) that the maximum angle between the tangent of the rod and the direction $\boldsymbol{AB}$ is larger than $\frac{\pi}{2}$.

-2- in the second region, under the $R = 2\pi$ curve, the curves of constant end-shortening and constant end-rotation never exhibit tangency. Hence the instability to self-contact will not occur here.

In a fixed-R experiment, the stability can be read from a particular diagram. Since R is constant, the only work done by the experimental device is the work of the tension

acting through the end-shortening d. Hence we eliminate m from (14) and (15) to get:

$$R = \frac{2}{\gamma}\sqrt{t}\sqrt{1-\frac{d^2\,t}{16}} + 4\arccos\sqrt{1-\frac{d^2\,t}{16}} \tag{17}$$

and use this to plot the tension against d (see fig. 5). In such a plot (called distinguished by certain authors [10] [18]), changes in stability will only happen at folds (and possibly bifurcation points). As stated in [16], in a rigid loading experiment following a vertical fold in fig. 5 in an anti-clockwise way has a destabilizing effect.

We then see that curves corresponding to end-rotation less that 2π present no (vertical) fold, hence the rod remains stable all along the path. Although the locus of the instability points (shown dashed in fig. 5) :

$$t = \frac{8}{d^2} + \frac{4\,\gamma}{d} \tag{18}$$

depends on γ, there is no change of qualitative behavior of the diagrams of fig. 4 & 5 with γ.

Yet another experiment can be devised : *Fixed D experiment* : keeping end-shortening fixed and tuning end-rotation. It would correspond to following curves of constant end-shortening in fig. 4. Using eqs. (14) and (15) and eliminating t, we find :

$$R_{\pm} = \frac{m}{\gamma} + 4\arccos\frac{m\,d}{2\sqrt{2}\,\sqrt{4\pm\sqrt{16-m^2\,d^2}}} \tag{19}$$

For this type of experiment, a distinguished diagram is obtained by plotting R against m and the destabilizing effect happens when following the fold in a clockwise way [11]. This is illustrated in fig. 6 where curves defined by eq. (19) with different values of d have been drawn together with the loci of the instability points defined by $\frac{\partial R_{\pm}}{\partial m} = 0$:

$$R = \frac{m}{\gamma} - \arctan\frac{m}{2\gamma} + 2\pi. \tag{20}$$

This curve (20) divides each path into a stable part (the part from $(m, R) = (0, 0)$ up to the R-fold) and an unstable one (the part from $(m, R) = (0, 2\pi)$ up to the R-fold).

The instability here is of the same nature as the one encountered before i.e. the rod will jump to self-contact. However, we see that not all the curves have a fold in R. Indeed calculating

$$\frac{\partial R_+}{\partial m}|_{m=0} = \frac{1}{\gamma} - \frac{d}{2}, \tag{21}$$

we find that curves with $d < \frac{2}{\gamma}$ have a self-contact jump instability, whereas curves with $d > \frac{2}{\gamma}$ have not.

In conclusion we see that the semi-finite correction introduced here makes the rod $L \lesssim \infty$ 'more stable' than the rod $L = \infty$, though they both exhibit the same type of instability : dynamic jump to self-contact, which in the semi-finite case depends on γ.

Finally we note that in principle, stability could be assessed using a dynamic approach, namely the amplitude equation introduced in [6] which has been used to study the stability (and more) of straight rods, helices and rings. But in the case of localised buckling, since the centre line is more complicated, this approach will be considerably more difficult.

4 Real finite computations

So far we have considered very long rods. This enabled us to associate the spatial configuration of the rod to the homoclinic orbit in the related phase space. This association was exact for an infinitely long rod and approximate for a very long rod. If we now want to treat in an exact way rods of finite length, we must look for other orbits in the phase space that fulfil the boundary conditions, since the homoclinic no longer does. Although there exist ways to write the solutions in closed form [14, 13, 15], we will compute them numerically and follow them as parameters are varied.

The first and main difference in this finite-length model is that we must consider negative tension (i.e. compression) : a straight, finite length rod can be stable under (sufficiently low) compression whereas an infinite rod would buckle as soon as placed

under compression. In fact the buckling curve $M^2 = 4T$ that holds when $L = \infty$ has to be replaced by the buckling curve for $L < \infty$ which, for clamped ends, is [7] :

$$\left(\cos\frac{1}{2}\sqrt{m^2-4t} - \cos\frac{m}{2}\right)\sqrt{m^2-4t} = t\,\sin\frac{1}{2}\sqrt{m^2-4t}\ ,\ \text{with}\ m^2 > 4t, \qquad (22)$$

where the same dimensionless variables have been used as in the previous section. Eq. (22) in fact defines a countable infinity of curves corresponding to increasingly higher buckling modes. In fig. 7 we have plotted the first three of these curves together with the curve $m^2 = 4t$ (bold). Notice that for a range of values of the twisting moment m, the rod buckles under compression. The condition for pure moment buckling ($t = 0$) : $\tan\frac{m}{2} = \frac{m}{2}$ can be found by Taylor expanding (22). The buckling curve $m^2 = 4t$ which holds for infinite length is valid for both clamped and pinned ends. In contrast, for a finite rod, different boundary conditions yield different buckling curves and different equilibrium configurations.

Since we no longer consider just the homoclinic orbits in the phase space but any orbit that fulfils the boundary conditions, the number of static configurations is larger and the post-buckling surface becomes more complicated [12]. Also, as shown in [7], the force vector no longer lies along the the $\boldsymbol{\ell}$ axis as it was in the infinite length case.

As done for the previous model, we will plot $D-T$ and $R-M$ distinguished diagrams to check the stability of the static configurations under fixed-R and fixed-D experiments respectively. Here D, for an arbitrary configuration, is given by (10). It takes values between 0 and $2L$ (for $D > L$ the rod leaves the clamps on the outside, see fig. 10). For details on the numerical techniques used we refer to [7].

Fixed R experiment : The $D - T$ response diagram for any finite-L rod with $\gamma = \frac{5}{7}$ is drawn in fig. 8. We see that bucking ($d \stackrel{\text{def}}{=} \frac{D}{L} = 0$) may happen for negative t (compression). We also note that as in fig. 5 not all the curves have a D-fold, which means that there are again two regimes for the curves emerging from the first buckling mode :

- for high end-rotation, $R > 2\pi$, there will be a jump to self-contact at a certain limiting d (see fig. 9),

- for low end-rotation, $R < 2\pi$, the buckled configurations are stable up to $d = 2$ (for the present value of γ), which includes, for $d > 1$, rod configurations with inverted clamps (see fig. 10). Change in the value of γ will qualitatively change the stability features of this experiment. For instance, we note that when γ is increased beyond $\sqrt{3}$, the curve with $R = 0$ acquires instability. This instability takes place at $d = 1$ when the rod forms a closed loop with one turn of twist put in. Since $\gamma = \sqrt{3}$ this implies that the twisting moment is $\sqrt{3}$, which is the buckling load for a planar ring [19]. The same argument can be used to show that curves with $0 < R \leq 2\pi$ will acquire instability for larger values of γ.

There are also some new curves in fig. 8, emerging from the second and third buckling modes. Hence just after buckling (i.e. for small d) they correspond to unstable configurations. But we see that some of these curves (the ones with $0 \leq R \leq 2\pi \left(\frac{\sqrt{3}}{\gamma} - 1\right)$ and $\gamma \leq \sqrt{3}$) are going through one (or more) stabilizing fold(s) at higher d. Hence for some values of R (at least the range $0 < R < 2\pi$) we will have intervals of D for which two stable configurations coexist.

Fixed D experiment : The $R - M$ response diagram for any finite-L rod with $\gamma = \frac{5}{7}$ is shown in fig. 11. We see that for small D, we have the same R-fold as before, i.e. an instability where the rod jumps to self-contact. But for larger values of D another fold appears, hence another instability takes place, for a smaller value of R. To understand what happens we consider the schematic representation in fig. 12. Let us choose a first point W on the stable part of the bifurcation curve and start decreasing the end-rotation of the rod (shapes are shown in fig. 13). After R has changed sign, we arrive at the new fold X. Trying to decrease further the end-rotation will cause the rod to jump, not to self-contact this time but to the other stable branch with positive m (point Y). Increasing R from there, we can reach another fold (point Z) to complete a symmetric hysteresis

path. When D is further increased, as in the semi-finite model, the R-fold corresponding to the self-contact instability disappears (see, e.g., the dotted curve in fig. 11). Finally, for yet higher D, the new folds (points Z and X of fig. 12) take place at $|R| > 2\pi$. This implies that we have again a jump to self contact.

Qualitative changes in the diagram of fig. 11 will happen if we vary γ [7]. Among others, when $\gamma > 1$ the fold corresponding to the self-contact instability will disappear before the hysteresis fold appears, which means that for some values of the end-shortening, static configurations of such a rod will be stable for all $R \in [0, 2\pi]$ and there will not be any jump at all.

5 Conclusion

In conclusion, we have seen that our three different approaches (infinite length, very large length, finite length) yield different results for the possible equilibrium configurations (and their stability) of a twisted rod subjected to clamped end conditions.

Experiments are envisaged by varying two independent displacements : the end-rotation R and the end-shortening D of the buckled rod.

The infinite length approach tells us that at low R and D the rod configuration is stable and that there is a limit curve

$$R = \frac{4}{\gamma\, d} \tag{23}$$

in the (R, D) plane at which the configuration loses stability and the rod jumps to self-contact (bold curve in fig. 14).

Introducing the semi-finite correction by considering a very large length instead of an infinite length yields a quantitative as well as a qualitative change in the stability curve which is now given by :

$$R = \frac{2}{\gamma}\sqrt{\frac{8}{d^2} + \frac{4\,\gamma}{d}}\,\sqrt{\frac{1}{2} - \frac{\gamma\, d}{4}} + 4\arccos\sqrt{\frac{1}{2} - \frac{\gamma\, d}{4}} \quad \text{for } d \in [\,0\,;\, d^\star] \tag{24}$$

where $d^\star \stackrel{\text{def}}{=} \frac{2}{\gamma}$. This curve is drawn plain in fig. 14 and it is easy to check that it has (23) for asymptote as $d \to 0$. Very long rods are more stable than infinite rods and hence jump to contact at higher displacements (R, D). Moreover at low R, very long rods are stable for all D. For $d > d^\star$, the curve (24) can be extended by the line $R = 2\pi$. When crossing this line, the rod, instead of jumping to self-contact, will smoothly touch itself.

Computations for a rod of finite length lead to the dashed curve of fig. 14. We can still define $d^\star$ as the value of d for which the curve reaches $R = 2\pi$. The dependence of $d^\star$ on γ for a finite length rod has first been derived in [19]. In fig. 14 the dashed curve has been scaled horizontally in order that the two $d^\star$ coincide. The finite length approach corrects the very long rod one by :

- pushing further the stability limit corresponding to the jump to contact (see the dashed curve of fig. 14),
- introducing new configurations, stable under compression, whose instability leads to a new kind of dynamic jump with the destabilized rod going to another contact-free configuration instead of self-contact.

These finite size effects which have been worked out here because the problem considered is amenable to analysis (1D elasticity) could help us to guess what are the stability features of other more complicated problems for which only the infinite length approach is available (2D elastic shells for example [9]).

References

[1] S. S. Antman, *Nonlinear Problems of Elasticity*, Springer-Verlag, Berlin, 1995.

[2] A. H. Cottrell, *The mechanical properties of matter*, Wiley, New York, 1964.

[3] J. Coyne, Analysis of the formation and elimination of loops in twisted cable, IEEE J. Ocean Eng. **15** (1990) pp 72-83.

[4] V. G. A. Goss, G. H. M. van der Heijden, J. M. T. Thompson and S. Neukirch, Experiments on snap buckling, hysteresis and loop formation in twisted rods, in preparation (2001).

[5] O. Gonzalez and J. H. Maddocks, Global Curvature, Thickness and the Ideal Shapes of Knots, Proc. National Academy of Sciences, USA 96 (1999) 4769-4773.

[6] A. Goriely and M. Tabor, New amplitude equations for thin elastic rods, Phys. Rev. Lett. 77 (1996) pp 3557-3540.

[7] G. M. H. van der Heijden, S. Neukirch, V. G. A. Goss and J. M. T. Thompson, Instability and self-contact phenomena in the writhing of clamped rods, in preparation (2001).

[8] G. H. M. van der Heijden and J. M. T. Thompson, Helical and localised buckling in twisted rods: a unified analysis of the symmetric case, Nonlinear Dynamics **21** (2000) pp 71-99.

[9] G.W. Hunt, M.A. Peletier, A.R. Champneys, P.D. Woods, M.A. Wadee, C.J. Budd, G.J. Lord, Cellular buckling in long structures, *Nonlinear Dynamics* **21**, 3-29 (2000).

[10] J. H. Maddocks, Stability and Folds, Arch. Rat. Mech. Anal. **99** (1987) pp 301-328.

[11] R. S. Manning, K. A. Rogers and J. H. Maddocks, Isoperimetric Conjugate Points with Application to the Stability of DNA Minicircles, Proc. R. Soc. Lond. A **454** (1998) pp 3047-3074.

[12] S. Neukirch and M. E. Henderson, Classification of the spatial clamped elastica, in preparation (2001).

[13] M. Nizette and A. Goriely, *Toward a classification of Euler-Kirchhoff filaments*, J. Math. Phys **40** (1999) pp 2830-2866.

[14] Y. Shi and J. E. Hearst, The Kirchhoff elastic rod, the nonlinear Schrödinger equation and DNA supercoiling, *J.Chem.Phys.* **101** (1994) pp 5186-5200.

[15] D. Swigon *Configurations with self contact in the theory of the elastic rod model for DNA* , Ph.D. dissertation, Rutgers State University of New Jersey, U.S.A. (1999).

[16] J. M. T. Thompson, Stability predictions through a succession of folds, Phil. Trans. R. Soc. Lond. A **292**, No 1386, (1979) pp 1-23.

[17] J. M. T. Thompson and A. R. Champneys, From helix to localised writhing in the torsional post-buckling of elastic rods, Proc. R. Soc. Lond. A **452** (1996) pp 117-138.

[18] H. Weinberger, *On the stability of bifurcating solutions*, Reprint from "Nonlinear Analysis" (dedicated to Erich Rothe), Academic Press (1978).

[19] E. E. Zajac, Stability of Two Planar Loop Elasticas, Transactions of the ASME Journal of Applied Mechanics **29** (1962) pp 136-142.

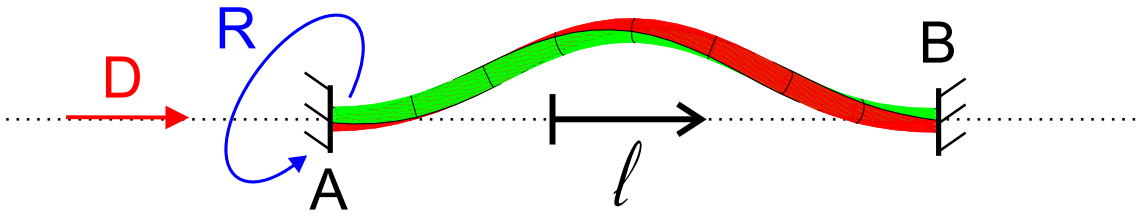

Figure 1: An elastic rod clamped at both ends. We experimentally control the distance $d(AB)$ by sliding the point A along $\boldsymbol{\ell}$, and the end-rotation R by turning the end of the rod at A around the axis $\boldsymbol{\ell}$.

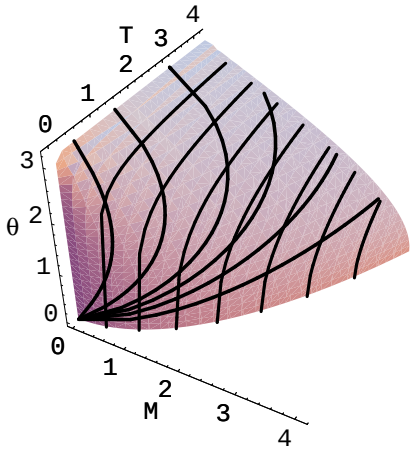

Figure 2: Post-buckling surface of an infinite twisted rod (eq. (11)). Curves of constant end-shortening D (eq. 10) and constant twisting moment M are shown.

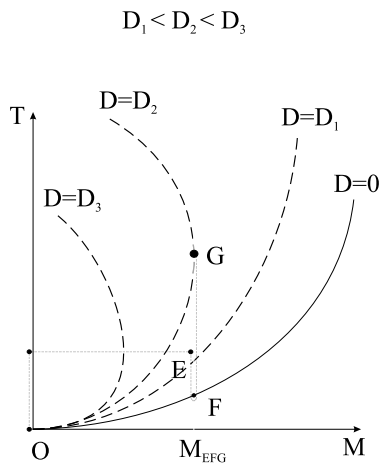

Figure 3: Path followed by the values of the tension T and twisting moment M along a typical fixed-R experiment. We start at point O and put the rod under tension and moment. At point E we let the tension decrease up to point F where the rod buckles. Then we follow a constant M path on the post-buckling surface up to point G where the spatial configuration becomes unstable. Note that since this diagram is a projection the paths EF and FG are not the same. $(M_G, T_G) = (\frac{4}{D_G}, \frac{8}{D_G^2})$.

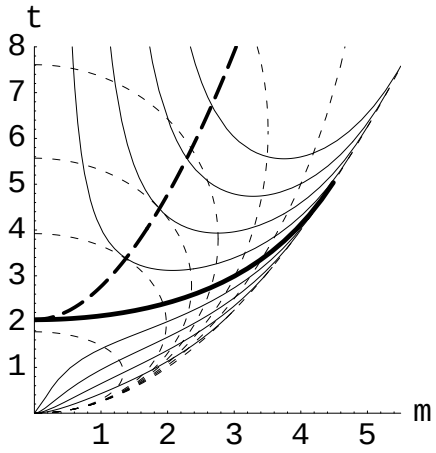

Figure 4: Projection of the post-buckling surface (fig. 2) on the m, t plane, for a very long twisted rod. Curves of constant end-shortening d (eq. (14)) are shown dashed. Curves of constant end-rotation R (eq. (15) with $\gamma = \frac{5}{7}$) are shown plain (the bold one corresponds to $R = 2\pi$). The curve of instability points is shown bold-dashed.

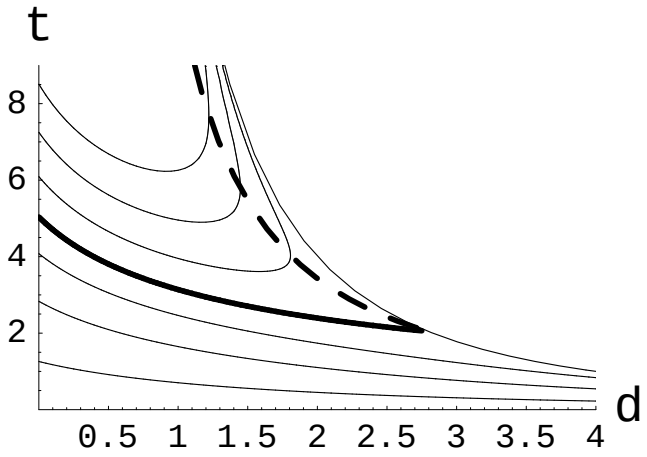

Figure 5: Response diagram for a very long twisted rod with $\gamma = \frac{5}{7}$ under constant end-rotation. Curves of constant R (eq. (17)) are shown (bold for $R = 2\pi$) together with the loci of instability points drawn as a dashed line (eq. (18)).

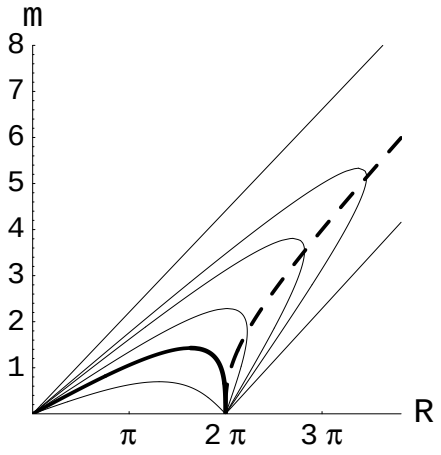

Figure 6: Response diagram for a very long twisted rod (with $\gamma = \frac{5}{7}$) under constant end-shortening. Curves (eq. (19)) are shown for $d = 0.051, 0.75, 1.05, 1.75, \frac{14}{5}$(bold), 5.739. The curve of instability points (20) is shown dashed.

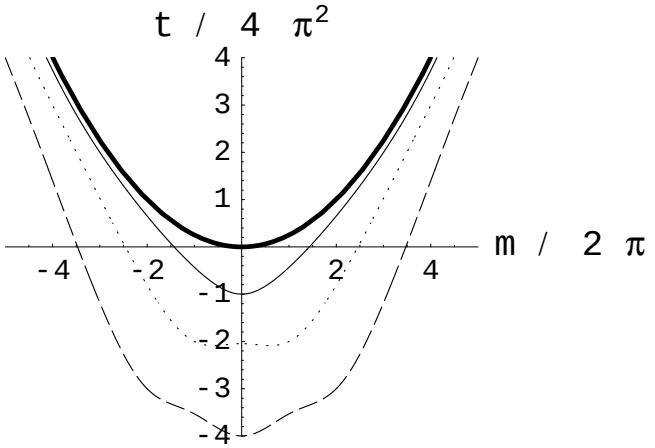

Figure 7: The bold curve is the buckling curve of an infinite length rod ($m^2 = 4t$) while the plain, dotted, dashed curves are the buckling curves of the 1st, 2nd and 3rd modes for a finite rod (eq. (22)). Traditional Euler compressive buckling is found at discrete points on the t axis.

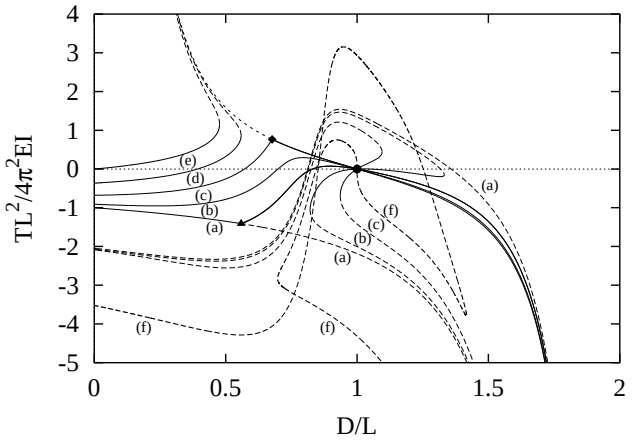

Figure 8: Response diagram for a twisted rod of arbitrary finite length L (with $\gamma = \frac{5}{7}$), at constant (positive) end-rotation. Curves are shown for $R = 0$ (a), $R = \pi$ (b), $R = 2\pi$ (c), $R = 3\pi$ (d), $R = 4\pi$ (e) and $R = 8.9$ (f). Rod configurations along plain (resp. dashed) curves are stable (resp. unstable).

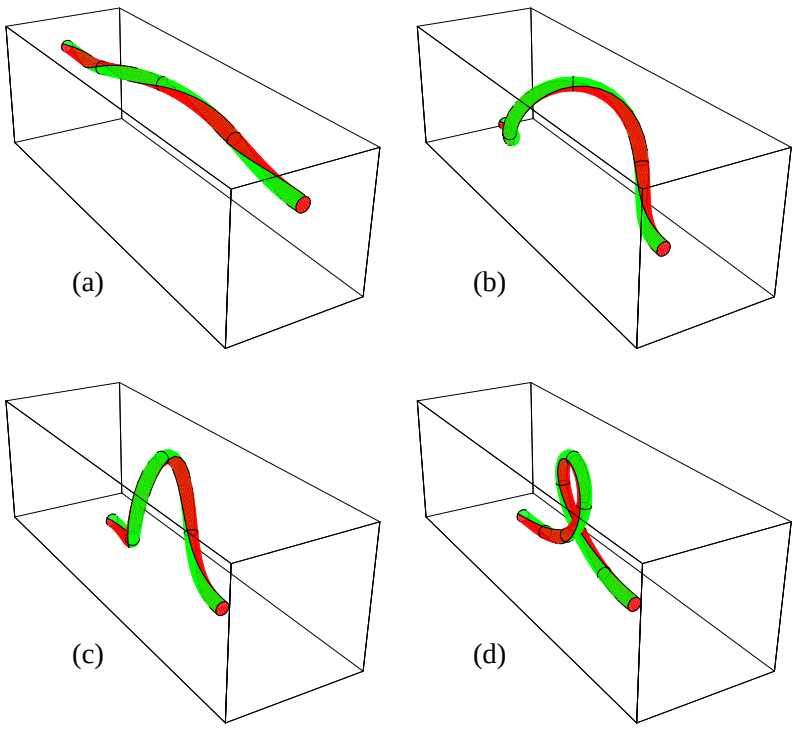

Figure 9: Shapes of a rod with $\gamma = \frac{5}{7}$ at constant $R = 11.4$ (radians) with slenderness ratio $\frac{L}{2\rho} = 10\pi$. (a) is for $d = 0.015$, just after the buckling instability. A loop starts to develop in (b) (for $d = 0.298$). Configurations just before and just after the dynamic jump (at $d = 0.504$) are shown in (c) and (d). Note that the jump happens after the maximum deflection angle has exceeded 90 degrees.

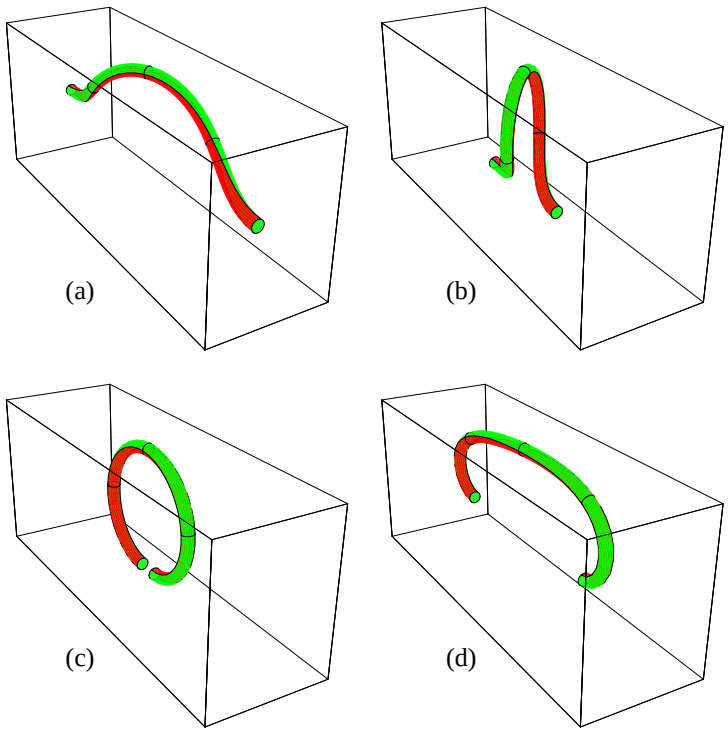

Figure 10: Shapes of a rod with $\gamma = \frac{5}{7}$ at constant $R = 4.265$ (radians). (a) is for $d = 0.115$, just after the buckling instability. A loop starts to develop in (b) (for $d = 0.69$), but no dynamic jump takes place. Instead, the rod reaches configurations in which the clamps are inverted, as in (c) ($d = 1.06$) and (d) ($d = 1.53$). Note that at $d = 1$ the rod forms a closed stable planar loop.

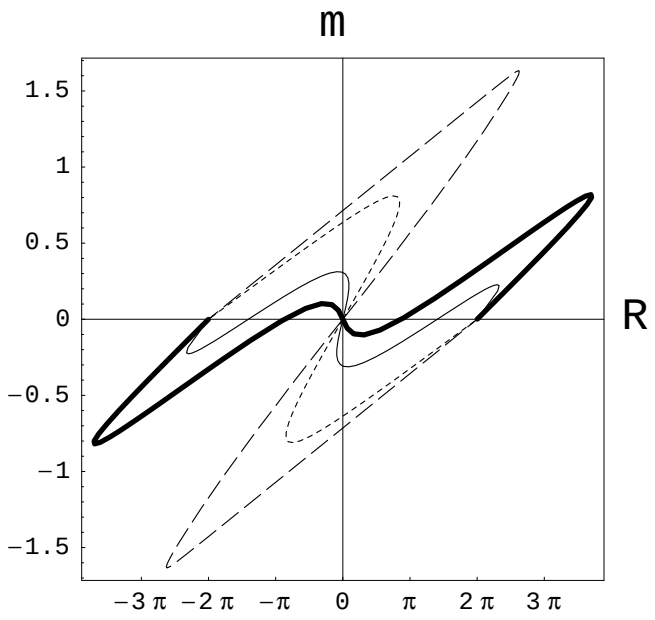

Figure 11: Response diagram for a twisted rod of arbitrary finite length L (with $\gamma = \frac{5}{7}$), at constant end-shortening. Curves are shown for $d = 0.5$ (bold), $d = 0.625$ (plain), $d = 0.8$ (dotted) and $d = 0.99$ (dashed).

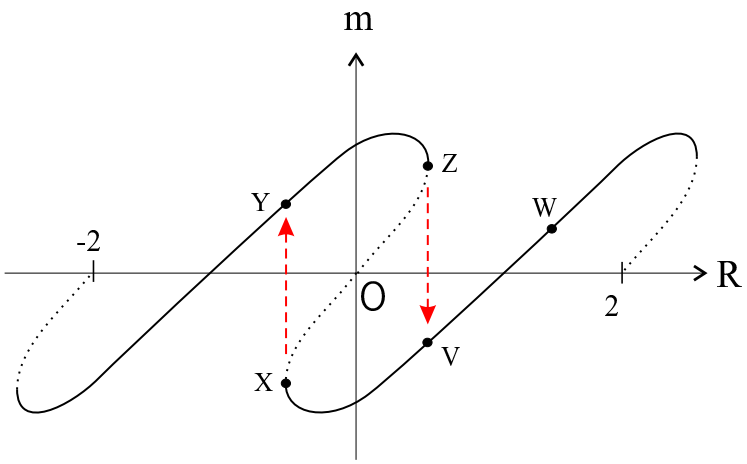

Figure 12: Schematic description of the hysteresis behaviour happening when tuning the end-rotation and keeping end-shortening fixed. Plain (dotted) lines indicate stable (unstable) rod configurations.

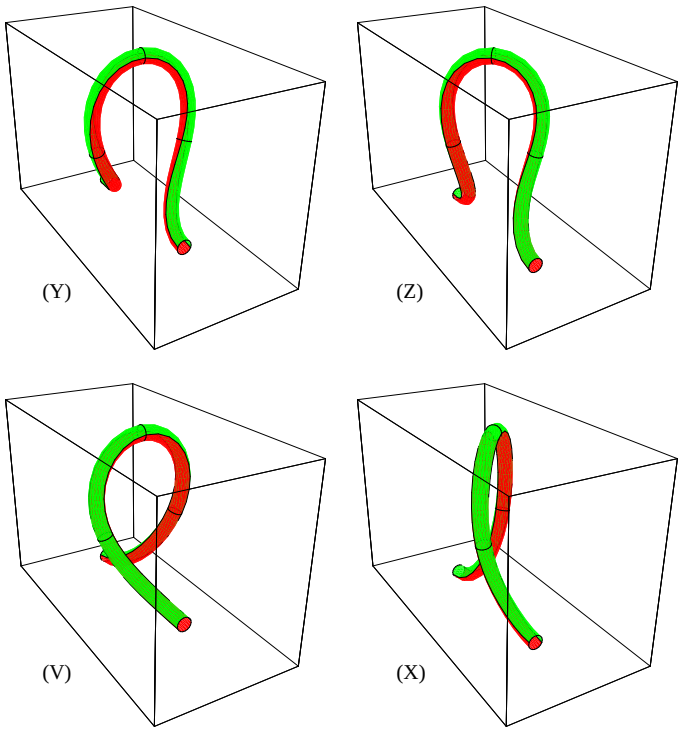

Figure 13: Shapes of a finite length rod ($\gamma = \frac{5}{7}$ and $\frac{L}{2\rho} = 10\pi$) along a constant $d = 0.67$ path. The four shapes correspond to the labels V, X, Y, Z of fig. 12.

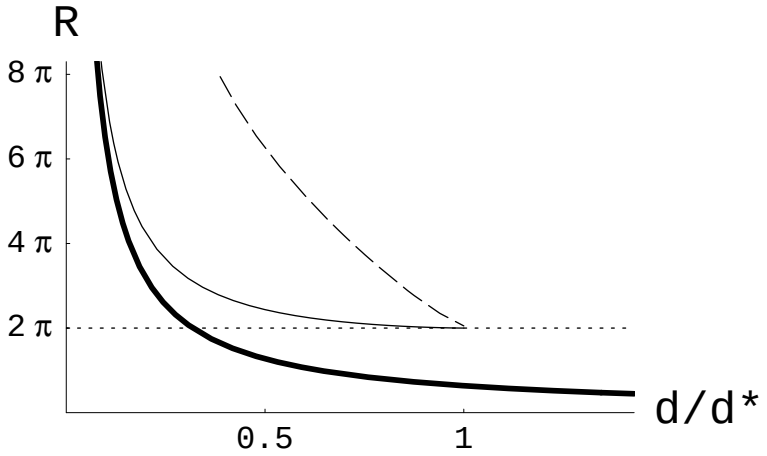

Figure 14: Stability diagram for $\gamma = \frac{5}{7}$ (hence $d^\star = 2.8$) for the 3 different models. The rod configuration is stable at low (R, D) and unstable at high values. The bold curve (eq. (23)) is for $L = \infty$, the plain curve (eq. 24) is for $L \lesssim \infty$ and the dashed curve is for arbitrary finite L.